ORIGINAL ARTICLE

AJT

Protection of liver sinusoids by intravenous administration of human Muse cells in a rat extra-small partial liver transplantation model

Yoshihiro Shono[1] | Yoshihiro Kushida[2] | Shohei Wakao[2] | Yasumasa Kuroda[2] | Michiaki Unno[1] | Takashi Kamei[1] | Shigehito Miyagi[1] | Mari Dezawa[2]

[1]Department of Surgery, Tohoku University Graduate School of Medicine, Sendai, Miyagi, Japan

[2]Department of Stem Cell Biology and Histology, Tohoku University Graduate School of Medicine, Sendai, Miyagi, Japan

Correspondence
Yoshihiro Shono and Shigehito Miyagi, Department of Surgery, Tohoku University Graduate School of Medicine, Sendai, Miyagi, Japan.
Email: shono@med.tohoku.ac.jp (Y. S.); msmsmiyagi@yahoo.co.jp (S. M.)

Mari Dezawa, Department of Stem Cell Biology and Histology, Tohoku University Graduate School of Medicine, Sendai, Miyagi, Japan.
Email: mdezawa@med.tohoku.ac.jp

Funding information
Grants-in-Aid for Scientific Research from the Ministry of Education, Science, and Culture of Japan, Grant/Award Number: 17K10504; Life Science Institute, Inc

Abstract

Small-for-size syndrome (SFSS) has a poor prognosis due to excessive shear stress and sinusoidal microcirculatory disturbances in the acute phase after living-donor liver transplantation (LDLT). Multilineage-differentiating stress enduring (Muse) cells are reparative stem cells found in various tissues and currently under clinical trials. These cells selectively home to damaged sites via the sphingosine-1-phosphate (S1P)–S1P receptor 2 system and repair damaged tissue by pleiotropic effects, including tissue protection and damaged/apoptotic cell replacement by differentiating into tissue-constituent cells. The effects of intravenously administered human bone marrow-Muse cells and -mesenchymal stem cells (MSCs) (4×10^5) on liver sinusoidal endothelial cells (LSECs) were examined in a rat SFSS model without immunosuppression. Compared with MSCs, Muse cells intensively homed to the grafted liver, distributed to the sinusoids and vessels, and delivered improved blood chemistry and Ki-67(+) proliferative hepatocytes and -LSECs within 3 days. Tissue clearing and three-dimensional imaging by multiphoton laser confocal microscopy revealed maintenance of the sinusoid continuity, organization, and surface area, as well as decreased sinusoid interruption in the Muse group. Small-interfering RNA-induced knockdown of hepatocyte growth factor and vascular endothelial growth factor-A impaired the protective effect of Muse cells on LSECs. Intravenous injection of Muse cells might be a feasible approach for LDLT with less recipient burden.

1 | INTRODUCTION

In living-donor liver transplantation (LDLT), the graft should be as small as possible for the donor, but as large as possible for the recipient.[1-4] Small-for-size syndrome (SFSS) in LDLT, a multifactorial disease caused by both donor and recipient factors, has a poor postoperative prognosis mainly due to sinusoidal microcirculatory disturbances after portal reflow.[5] Prophylactic measures against SFSS are represented by portosystemic shunts, splenectomy to modulate portal pressure, splenic arterial ligation/embolization, somatostatin and its analogs, and larger graft selection based on the graft-to-recipient weight ratio (GRWR), but no effective treatments have been established.[6-11] In rats with SFSS, treatment with stem cells such as mesenchymal stem cells (MSCs) and adipose-derived stem cells is reported to be effective.[12-14]

Liver regeneration is a remarkable physiologic reaction after LDLT, hepatectomy, and liver injury, promoted by various signaling pathways involving extracellular matrix remodeling, metabolites, tumor necrosis factor-α, interleukin-6, and bile acids.[15-19] In SFSS, liver sinusoidal endothelial cells (LSECs) are injured by shear stress after portal reflow. Shear stress is, in a sense, a necessary trigger for inducing smaller grafts to regenerate their original volume in the early stages of liver regeneration.[20-23] While moderate shear stress beneficially affects LSECs and liver regeneration, excessive shear stress disturbs liver regeneration.[24] Serious vascular endothelial damage during the early postoperative period negatively affects graft survival and prognosis. If an effective and easily accessible treatment for sinusoidal microcirculatory disturbances can be established, smaller grafts can regenerate after transplantation, allowing for reduced graft volume with a high graft survival rate. This may contribute to decrease the donor shortage, extend donor adaptation, and reduce the donor burden.

Multilineage-differentiating stress enduring (Muse) cells are non-tumorigenic endogenous pluripotent-like stem cells, identified as cells positive for the pluripotent stem cell surface marker stage specific embryonic antigen (SSEA)-3, present in the bone marrow (BM), peripheral blood, and connective tissues of organs.[25-28] They can also be harvested from cultured MSCs as several percent of the total cell population.[29,30] Muse cells have several unique properties: (1) intravenously injected Muse cells recognize damaged tissue and selectively accumulate at the site of damage because they express the sphingosine-1-phosphate (S1P) receptor 2, which recognizes the S1P produced by damaged/apoptotic cells; and (2) after selective homing to the damaged site, Muse cells replace damaged/apoptotic cells by spontaneous differentiation into the damaged/apoptotic cell type, and contribute to tissue repair.[31] In murine models of fulminant hepatitis, hepatectomy, and cirrhosis, intravenously injected human Muse cells spontaneously differentiate into liver components, such as hepatocytes, sinusoidal endothelium, bile duct epithelium, and Kupffer cells, after homing to the damaged liver.[32,33]

Besides tissue repair effects, Muse cells have other beneficial effects, such as neovascularization, immunomodulation, trophic-, anti-apoptotic-, and anti-fibrotic effects.[33-35] Furthermore, allogeneic-Muse cells escape host immunorejection after intravenous administration and survive in the host tissue as differentiated cells for over 6 months, even without immunosuppressive treatment.[31] This ability is partly explained by the expression of human leukocyte antigen (HLA)-G, a histocompatibility antigen that mediates immune tolerance in the placenta.[31] In fact, intravenously administered allogeneic-Muse cells have been applied to clinical trials under the approval of regulatory authorities for acute myocardial infarction, stroke, epidermolysis bullosa, spinal cord injury, and neonatal hypoxic-ischemic encephalopathy without HLA matching or long-term immunosuppressants.[36,37]

In the present study, we created a rat model of LDLT with an extra-small graft to partially mimic clinical SFSS, and human Muse cells were intravenously administered soon after transplantation without immunosuppression. Human BM-MSCs were used as a control because MSCs contain Muse cells and their effectiveness in SFSS was previously evaluated in rats.[12-14] In clinical LDLT, the prognosis of the grafted liver is significantly affected by portal hypertension for 4 days after transplantation.[38] In rat partial liver transplantation, liver regeneration begins immediately after portal reflow, with the production of regenerative factors diminishing by day 7 after transplantation.[39,40] Therefore, our study focused on evaluating the 3 days after Muse cell administration.

2 | MATERIALS AND METHODS

2.1 | Preparation of human BM-MSCs and Muse cells

Human BM-MSCs were purchased from Lonza (Cat. # PT-2501). SSEA-3(+) human Muse cells were collected from human BM-MSCs as SSEA-3(+) by magnetic-activated cell sorting as described.[35,41,42] Collected cells were cultured overnight to exclude dead cells, and then suspended in cryopreservation solution (Cat. # ZR638, Zenoaq) and stored at −80°C until use.

2.2 | Rat extra-small partial liver transplantation model

Male Lewis rats, weighing 270–300 g, aged 10–13-week-old were purchased from Japan SLC, Inc. All experiments were conducted

according to the Guide for the Care and Use of Laboratory Animals prepared by the National Academy of Sciences and published by the National Institutes of Health. The study was approved by the Animal Care and Use Committee of Tohoku University.

Extra-small partial liver transplantation was performed according to the cuff method for portal vein reconstruction with re-arterialization.[39,43-45] The 20% liver graft comprised the superior right lobe and inferior right lobe. The details are provided in the Supplemental Methods. Portal pressure was directly measured using a saline manometer after all reconstruction.

Animals received an injection of cells suspended in 2 ml saline via the penile vein within 2.5 h after portal reflow because reconstruction of the infrahepatic inferior vena cava, artery, and biliary duct required ~2.5 h, and because cells freshly recovered from cryopreservation were considered preferable for injection.

2.3 | Animal groups

Operated rats were divided into five groups, receiving either saline (vehicle group), 0.4 million BM-MSCs (MSC-0.4M group), 5 million BM-MSCs (MSC-5M group), 0.4 million Muse cells (Muse group), or 0.4 million hepatocyte growth factor (HGF)/vascular endothelial growth factor A (VEGFA)-knocked down-Muse cells (HGF/VEGF-KD-Muse group). The intact group comprised naïve animals that did not undergo any procedures. Portal pressure was measured in animals that underwent whole liver transplantation.

Ten animals were used for GRWR, indocyanine green (ICG) test, blood biochemistry and terminal deoxynucleotidyl transferase deoxyuridine triphosphate nick-end labeling (TUNEL) staining, and five animals were used for portal flow pressure measurement, evaluating the dose dependency of Muse cells, in vivo dynamics of Akaluc-labeled cells, sinusoidal imaging, and immunohistochemistry.

2.4 | ICG test and blood biochemistry

The ICG test was performed as described previously.[46] The data for the intact group are not shown in the figures because the values differed greatly from those of the experimental groups. Blood samples were analyzed by DRI-CHEM 7000V (Fujifilm) at day 3.

2.5 | In vivo dynamics of intravenously injected cells

BM-MSCs were infected with Akaluc/pcDNA3 lentivirus,[47] and then SSEA-3(+)-Muse and SSEA-3(–)-MSCs (named "non-Muse cells") were separated by fluorescence-activated cell sorting. After separation, the Akaluc-labeled Muse and non-Muse cells were mixed at a ratio of 7:3 to mimic the ratio of Muse cells in the Muse group.

At day 3, the rats were administered 1 mg AkaLumine-HCl (6.6 mM, Cat. #035-22991, FUJIFILM Wako Pure Chemical

Corporation) in distilled water. Each organ was removed and immersed in 500 μM AkaLumine-HCl in normal saline, and evaluated using an IVIS Spectrum CT in vivo imaging system (Perkin Elmer).

2.6 | Tissue clearing and sinusoidal imaging

At day 3, rats were administered 1 mg/ml Texas Red-labeled dextran dissolved in phosphate-buffered saline (Cat. #D1864, Thermo Fisher) at 1 mg/100 g body weight via the penile vein. Texas Red-dextran is lysine fixable, and thus the signal remained in the vessel after fixation. Five minutes later, the graft liver was removed, fixed by 4% paraformaldehyde, subjected to tissue clearing and was observed under multiphoton laser confocal microscopy (A1 MP+, Nikon) to obtain three-dimensional (3D) images.

Detailed methods are provided in the Supplemental Methods.

3 | RESULTS

3.1 | Study condition for intravenous administration of human Muse cells

The mean percent of Muse cells in BM-MSCs was 6.3 ± 1.7% (Figure S1). Magnetic-activated cell sorting yielded 73.0 ± 2.7% Muse cells, similar to previous reports (Figure S1).[35,41,42] Isolated Muse cells with a Muse cell ratio less than 70% were not used in the experiments.

Extra-small partial liver transplantation was performed in rats as shown in Figure 1A. A representative liver graft after anastomosis is shown in Figure 1B. Approximately 5.26% of the rats died within 48 h after surgery, whereas the survival rate beyond 48 h was 100%. Mortality did not differ among the experimental groups within 48 h. Rats with biliary complications were excluded.

Portal pressure did not differ between the hepatic (16.38 ± 1.12 cm H_2O) and enteral (16.32 ± 1.15 cm H_2O; $p = .94$) sides of the portal cuff. When the whole liver was transplanted, however, the portal pressure on the hepatic side was 10.58 ± 1.01 cm H_2O, which was significantly lower than that in the 20% liver transplantation ($p < .001$). At day 3, the patency of the reconstructed portal vein and hepatic artery was visually confirmed in all rats. Biliary complications were not detected in the analyzed rats.

To determine the optimal dose of Muse cells for intravenous injection, an ICG test was performed. While human Muse cells were injected to rat models, none of the animals underwent immunosuppression in the following experiments.

The ICG-plasma disappearance rate (PDR) of intact rats was 0.21 ± 0.02 and that of the vehicle group was 0.033 ± 0.009. The ICG-PDR of groups injected with 1×10^5, 2×10^5, and 4×10^5 Muse cells was 0.032 ± 0.012, 0.055 ± 0.021, and 0.068 ± 0.018, respectively. The ICG-PDR differed significantly between the 1×10^5- and 4×10^5-Muse cell groups ($p = .0095$), and between the vehicle and 4×10^5-Muse cell groups ($p = .012$; Figure 1C). Although there was no significant difference between 2×10^5 and 4×10^5 Muse cells
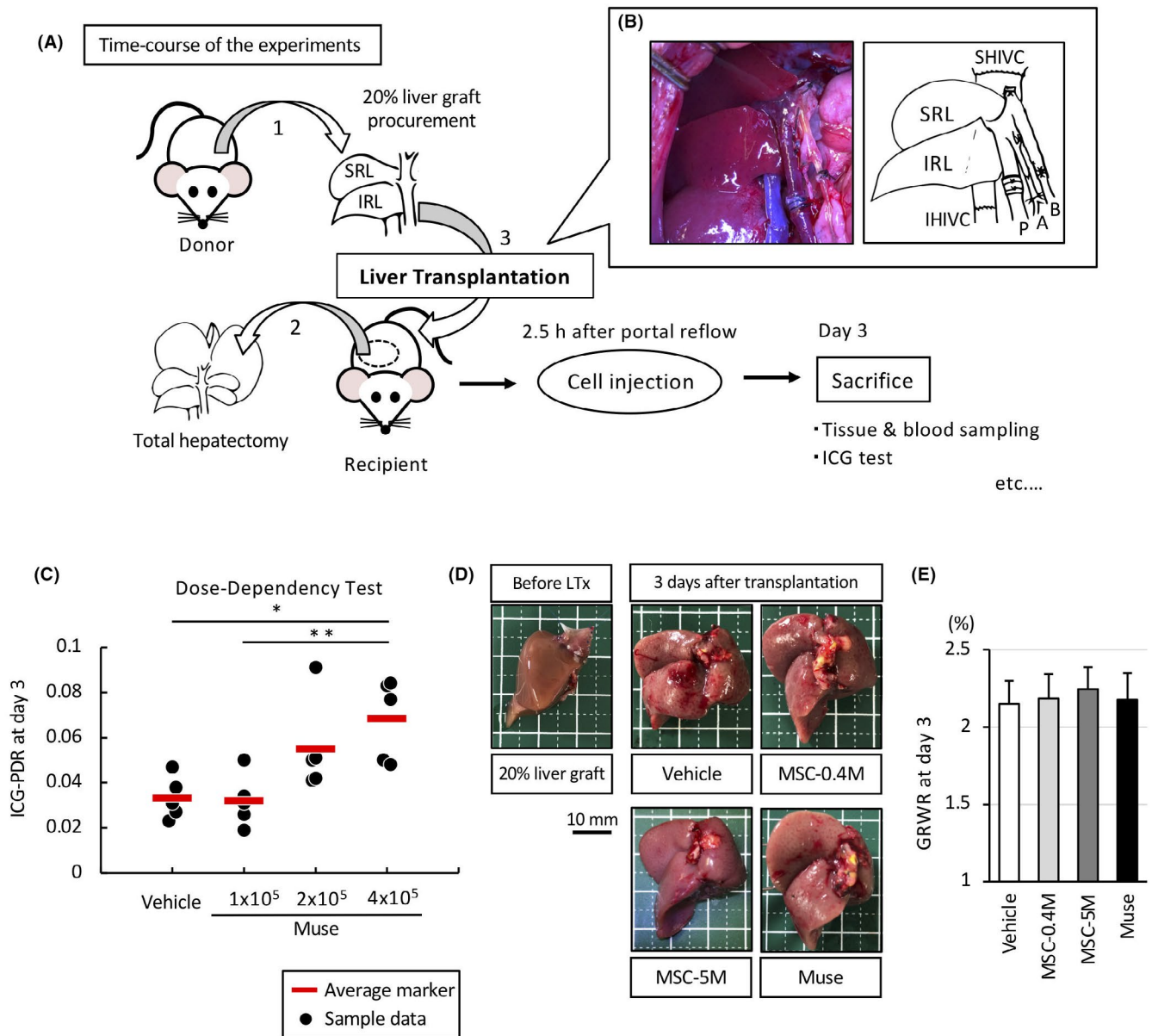
FIGURE 1 Experimental outline and dose-dependency test by ICG. (A) Schema and time course of the experiments. Volume reduction was performed in the donor whole liver. A 20% liver graft composed from the SRL and IRL was transplanted to the recipient after removing the recipient's whole liver. (B) Representative liver graft image and a contour-traced image after anastomosis. (C) To determine the best dose of Muse cells for intravenous injection, an ICG plasma clearance test was performed in the vehicle and 1×10^5, 2×10^5, and 4×10^5 Muse cell groups ($n = 5$/group). Mean ICG-PDR in intact rats was 0.21 ± 0.02. (D) Representative images of liver grafts before and 3 days after cell injection in each group. Sizes and appearance of the liver grafts did not differ significantly. (E) GRWR did not differ significantly among the four groups ($n = 10$/group). *$p < .05$, and **$p < .01$. A, hepatic artery; B, bile duct; GRWR, graft-to-recipient weight ratio; ICG, indocyanine green; IHIVC, infrahepatic inferior vena cava; IRL, inferior right lobe; LTx, liver transplantation; MSC, mesenchymal stem cell; Muse, Multilineage-differentiating stress enduring; P, portal vein; PDR, plasma disappearance rate; SHIVC, suprahepatic inferior vena cava; SRL, superior right lobe

($p = .54$), we decided to inject 4×10^5 Muse cells as the "Muse group" in the following experiments because the ICG-PDR of 4×10^5 Muse cells was better than that of 2×10^5 Muse cells (Figure 1C).

Because the Muse group received 4×10^5 cells, the same number of human BM-MSCs was injected for the MSC group ("MSC-0.4M group"). We also used another MSC group that received 5×10^6 BM-MSCs ("MSC-5M group"); this group received MSCs containing the same number of Muse cells as the Muse group. As mentioned

above, the purity of the Muse cell population after isolation by magnetic-activated cell sorting was ~73%. Therefore, the 4×10^5-Muse cell population used for the Muse group contained ~3×10^5 pure Muse cells. Because the proportion of Muse cells in MSCs is ~6.3%, 5×10^6 MSCs contain ~3×10^5 Muse cells.

At 3 days after cell injection, the size and appearance of the grafted livers did not differ among the four groups (Figure 1D). The GRWR also did not differ significantly among the four groups (Figure 1E).

3.2 | ICG-PDR

The ICG-PDR, an indicator of dynamic liver function, was 0.036 ± 0.010 in the vehicle group, 0.042 ± 0.011 in the MSC-0.4M group, 0.047 ± 0.020 in the MSC-5M group, and 0.068 ± 0.018 in the Muse group (Figure 2A). ICG-PDR was significantly different between the Muse and MSC-5M groups (p = .0262), Muse and MSC-0.4M groups (p = .0033), and Muse and vehicle groups (p = .0003), with the highest recovery of ICG-PDR in the Muse group. ICG-PDR was not significantly different between the vehicle and MSC-0.4M (p = .84) or MSC-5M (p = .38) groups, or between the MSC-0.4M and MSC-5M groups (p = .86).

3.3 | Blood biochemistry analysis

The Muse group had significantly lower aspartate transaminase (AST, p = .0356) and alanine transaminase (ALT, p = .0395) levels than the vehicle group (Figure 2B). While the Muse group tended to have lower ammonia, γ-glutamyl transpeptidase, and total bilirubin values, and a higher albumin value compared with the vehicle, MSC-0.4M, and MSC-5M groups, these parameters did not differ significantly among the four groups (Figure 2B). Notably, the values of these parameters in the MSC-0.4M and MSC-5M groups were similar with no significant differences between them (Figure 2B).

Because the MSC-0.4M and MSC-5M groups had approximately the same values and showed no significant difference in ICG-PDR and blood biochemistry, the MSC-0.4M group was selected as representative of the two MSC groups in the following experiments.

3.4 | In vivo dynamics of intravenously injected Akaluc-Muse cells and -MSCs

In the Muse group, the Akaluc signal was detected in the liver graft at 3 days after administration, while it was under the detection limit in the other organs, except the lung, which was the first capillary trap after intravenous injection (Figure 3A). In the MSC-0.4M group, significantly less Akaluc signal was detected in the grafted

FIGURE 2 The ICG-PDR and blood biochemistry analysis. (A) ICG-PDR after vehicle, MSC-0.4M, MSC-5M, and Muse cell administration (n = 10/group). The Muse cell group exhibited the highest ICG-PDR recovery. (B) Blood biochemistry analysis (n = 5 for intact rats, n = 10/group for the other four groups). Statistical analysis was performed among the vehicle, MSC-0.4M, MSC-5M, and Muse groups. *p < .05, **p < .01, and ***p < .001. ALB, albumin; ALP, alkaline phosphatase; ALT, alanine transaminase; AST, aspartate transaminase; ICG-PDR, indocyanine green plasma disappearance rate; Muse, multilineage-differentiating stress enduring NH$_3$, ammonia; T-Bil, total bilirubin; γ-GTP, γ-glutamyl transpeptidase
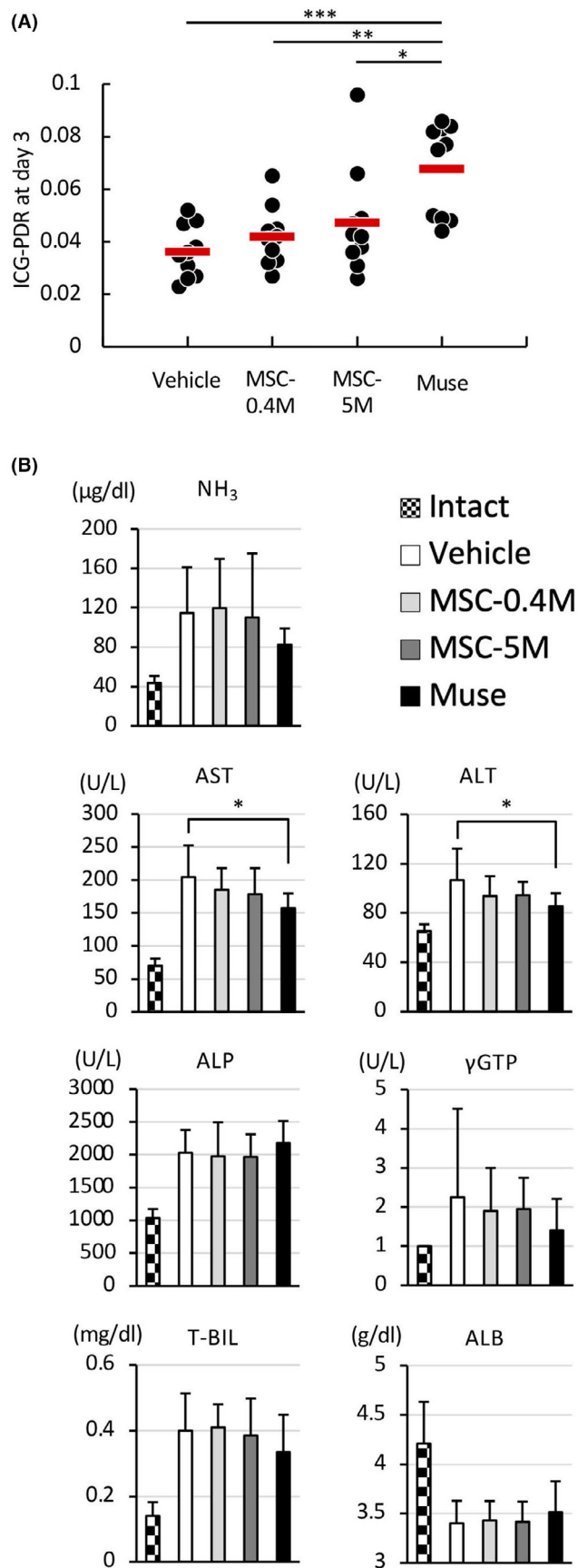
liver compared with the Muse group and except for the lung, the Akaluc signal was under the detection limit in the other organs (Figure 3B).
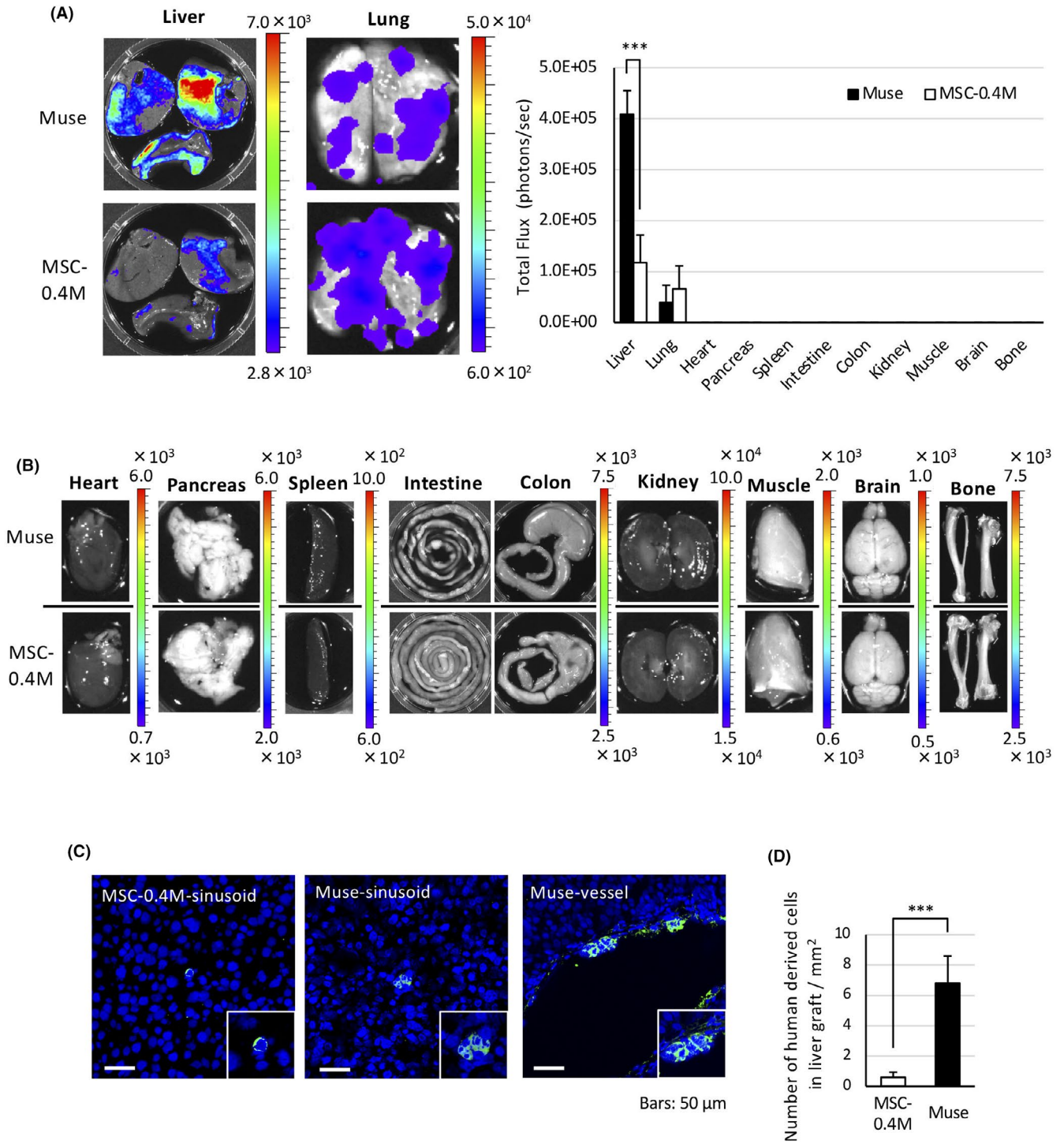
FIGURE 3 In vivo dynamics of intravenously injected Muse cells and MSCs. (A) Three days after intravenous administration, the Akaluc signal was detected predominantly in the liver graft in the Muse group while it was weaker in the MSC group (n = 5/group). (B) In the other organs, except for the lung (the first capillary trap after intravenous injection), the Akaluc signal was under the detection limit. (C) Representative images of STEM121, a human-specific cytoplasmic marker, at 3 days after intravenous administration. Blue shows DAPI signals (nuclear counterstain) and green shows STEM121 signals. (D) STEM121 was detectable in the liver graft of both the Muse and MSC-0.4M groups with significantly higher levels in the Muse group than in the MSC-0.4M group. MSCs were mainly detected in sinusoids while Muse cells were detected in both sinusoids and larger vessels. Bars: 50 µm, n = 5/group, *p < .05, **p < .01, and ***p < .001. DAPI, 4′,6-diamidino-2-phenylindole; MSCs, mesenchymal stem cells; Muse, multilineage-differentiating stress enduring; STEM121, human-specific cytoplasmic marker
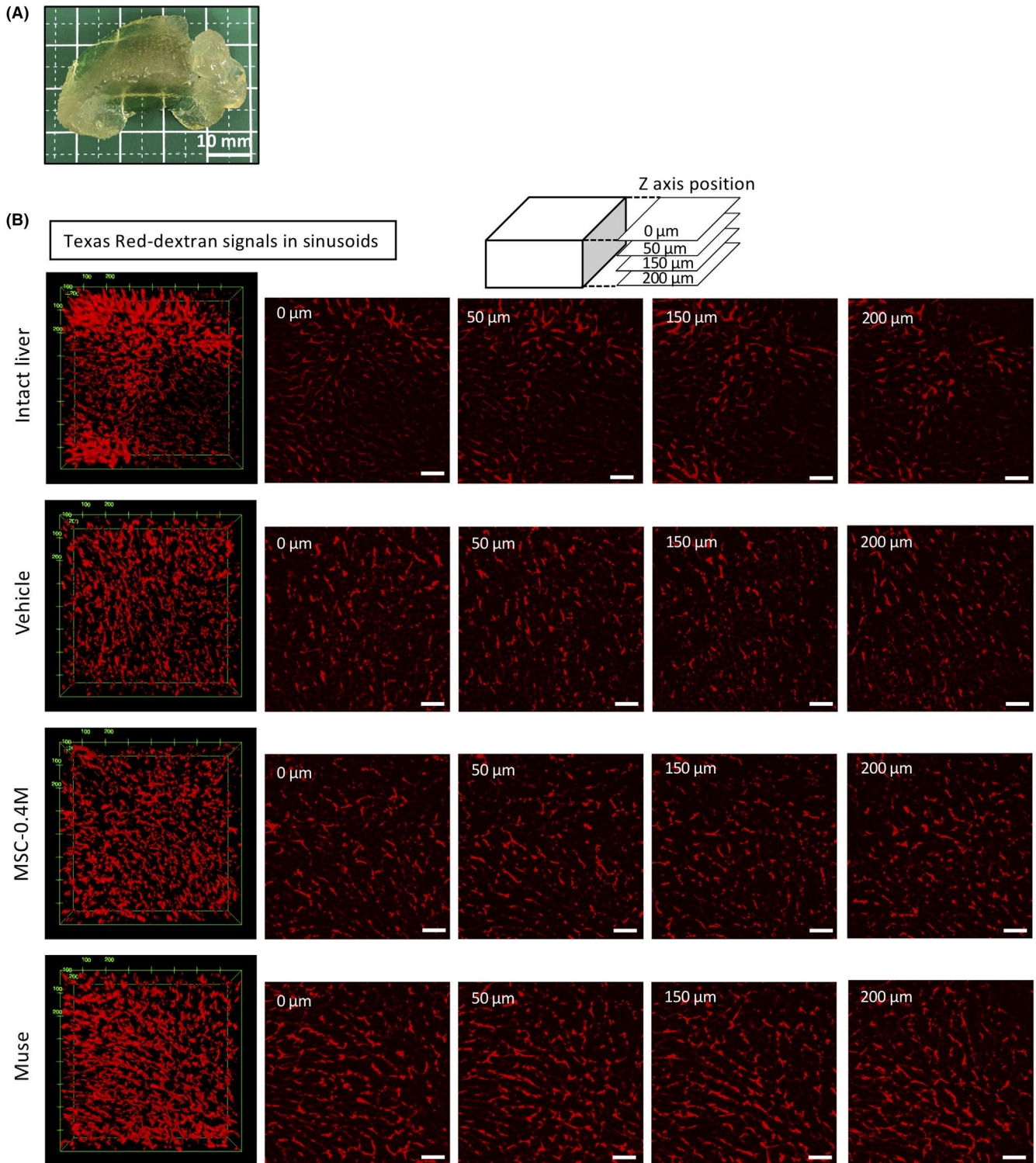
FIGURE 4 Liver sinusoidal images obtained from cleared liver tissues. (A) Example of a cleared liver in the vehicle group. (B) 3D frames of movies and 2D-images exported from the 3D images at every 50-μm Z-axis level (*n* = 5/group). Compared with sinusoids in the intact group, those in the vehicle and MSC-0.4M groups were irregularly organized and interrupted. Sinusoids in the Muse group, however, were continuous, similar to those in the intact group. The size of the rectangle in the 3D images is X: 795.5 μm × Y: 795.5 μm × Z: 200.6 μm. Bars in (A): 10 mm, bars in (B): 100 μm. 2D, two-dimensional; 3D, three-dimensional; MSC, mesenchymal stem cell; Muse, multilineage-differentiating stress enduring

In immunohistochemistry, STEM121, a human-specific cytoplasmic marker, was detectable in the liver grafts of the Muse and MSC-0.4M groups, but the frequency was significantly higher in the Muse group (6.80 ± 1.79 cells/mm^2) than in the MSC-0.4M group (0.60 ± 0.33 cells/mm^2; $p < .001$; Figure 3C,D). Notably, STEM121(+) cells were detected in the sinusoids and larger vessels

in the Muse group, but only in the sinusoids in the MSC-0.4 group (Figure 3C).

These findings suggested that Muse cells homed to and incorporated into the grafted liver more efficiently than MSCs within 3 days after administration.

3.5 | Evaluation of the sinusoid protection effect

The 3D images of the sinusoids were obtained from each group at 3 days. Because the dextran was injected intravenously, the liver sinusoids were selectively depicted. Figure 4A shows an example of a cleared liver in the vehicle group. Figure 4B shows 3D frames of movies (Movie S2A, C, E, G) and 2D images exported from the 3D images at every 50-μm Z-axis level. Compared with the sinusoids in the intact group, those in the vehicle and MSC-0.4M groups were irregularly organized and interrupted. Sinusoids in the Muse group, however, were continuous, similar to those in the intact group (Figure 4B).

The detailed organization of the sinusoids was further analyzed using the Gaussian Blur 3D, Median Filter 3D, and 3D Objects Counter plug-ins for ImageJ. Each continuous sinusoid was colored a distinct color by Glasbey-on-dark processing (Movie S2B, D, F, H). Continuous sinusoids were more abundant in the liver in the intact and Muse groups, whereas the majority of sinusoids in the vehicle and MSC-0.4M group liver grafts were discontinuous (Figure 5A).

The ratio of the total liver sinusoidal volume per unit volume was significantly higher in the Muse group (6.35 ± 0.28%) than in the vehicle (3.16 ± 0.88%; $p < .0001$) and MSC-0.4M (3.29 ± 0.38%; $p < .0001$) groups (Figure 5B). Notably, there was no significant difference between the Muse and intact groups (6.16 ± 0.10%, $p = .9313$; Figure 5B).

The mean continuous sinusoidal volume within one field of view was significantly higher in the Muse group (164 113 ± 23 081 μm^3) than in the intact (77 392 ± 17 156 μm^3; $p < .0001$), vehicle (35 578 ± 26 961 μm^3; $p < .0001$), and MSC-0.4M groups (35 134 ± 7204 μm^3; $p < .0001$; Figure 5C).

The mean continuous sinusoid surface area, namely the luminal surface area of the sinusoids, was also significantly higher in the Muse group (77 860 ± 17 299 μm^2) compared with the intact

(42 003 ± 5712 μm^2; $p = .0004$), vehicle (17 369 ± 10 579 μm^2; $p < .0001$), and the MSC-0.4M groups (18 098 ± 3605 μm^2; $p < .0001$; Figure 5D).

The number of interrupted sinusoids was significantly lower in the Muse group (135 ± 30) than in the vehicle (289 ± 53; $p = .0001$) and MSC-0.4M (311 ± 55; $p < .0001$) groups. The Muse and intact (176 ± 17) groups were not significantly different ($p = .44$), while the number of interrupted sinusoids was significantly higher in the MSC-0.4M ($p = .0006$) and vehicle groups ($p = .0030$) than in the intact group (Figure 5E).

3.6 | Immunohistochemistry for LSECs and Ki-67

Immunohistochemistry for lymphatic vessel endothelial hyaluronan receptor 1 (lyve-1), a surface marker for LSECs, revealed that the percent positive area was significantly higher in the Muse group (4.13 ± 0.22%) compared with the vehicle (2.19 ± 0.39%; $p < .001$) and MSC-0.4M (2.30 ± 0.11%; $p < .001$) groups (Figure 6A,D), but did not differ significantly between the Muse and intact (4.00 ± 0.22%) groups ($p = .87$; Figure 6D).

The Ki-67 positivity, indicating proliferative activity in hepatocytes, was significantly greater in the Muse group (56.51 ± 4.07%) than in the vehicle (46.21 ± 1.04%, $p < .001$) and MSC-0.4M groups (48.28 ± 1.45%; $p < .001$; Figure 6B,E).

The hepatic sinusoidal endothelial cells antibody (SE-1) is another surface marker for LSECs. SE-1 and Ki-67 double-positivity, indicating proliferating LSECs, was significantly higher in the Muse group (26.2 ± 3.5%) than in the vehicle (16.3 ± 1.2%, $p < .001$) and MSC-0.4M groups (18.5 ± 2.3%; $p = .0011$, Figure 6C,F).

3.7 | The LSEC protection effects of HGF/VEGF-KD-Muse cells

HGF and VEGFA are involved in LSEC protection.[48] The gene expression level of HGF and VEGFA was substantially higher in Muse cells than in MSCs; HGF was 2.84 ± 0.051 times higher ($p < .001$) and VEGFA was 2.08 ± 0.055 times higher ($p < .001$) in Muse cells than in MSCs in quantitative polymerase chain reaction (qPCR) (Figure 7A). We then estimated how these factors contribute to the protective

FIGURE 5 Evaluation of the sinusoid protection effect. (A) Glasbey-on-dark processing was used to color each continuous sinusoid with a distinct color to clarify the detailed organization of the sinusoids. Continuous sinusoids were more abundant in the liver of the intact and Muse groups, while the majority of sinusoids in the liver grafts were discontinuous in the vehicle and MSC-0.4M groups. (B) The ratio of the total liver sinusoidal volume per unit volume was higher in the Muse group than in the vehicle and MSC-0.4M groups ($n = 5$/group). The difference between the Muse and intact groups was not significantly different. (C) The mean continuous sinusoidal volume within one field of view was significantly higher in the Muse group than in the intact, vehicle, and MSC-0.4M groups ($n = 5$/group). (D) The mean continuous sinusoid surface area, namely the luminal surface area of the sinusoids, was also significantly higher in the Muse group compared with the intact, vehicle, and MSC-0.4M groups ($n = 5$/group). (E) The number of interrupted sinusoids was significantly lower in the Muse group than in the vehicle and MSC-0.4M groups ($n = 5$/group). There was no significant difference between the Muse and intact groups. The size of the rectangle in the 3D images is X: 795.5 μm × Y: 795.5 μm × Z: 200.6 μm. Bars: 100 μm, *$p < .05$, **$p < .01$, and ***$p < .001$. 2D, two-dimensional; 3D, three-dimensional; MSC, mesenchymal stem cell; Muse, multilineage-differentiating stress enduring

(A)

Color-coded signals for continuous sinusoids

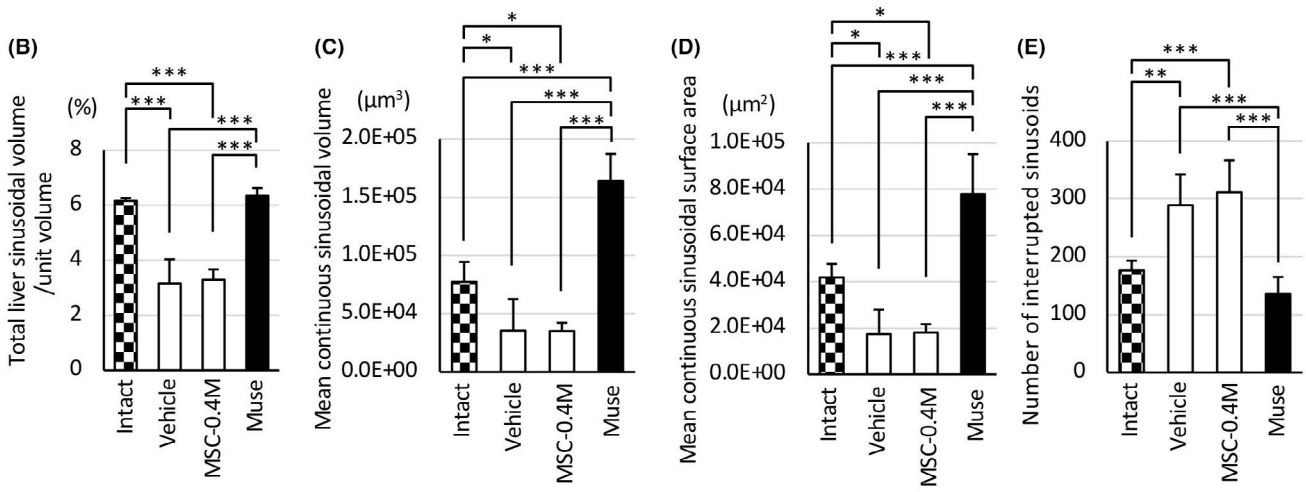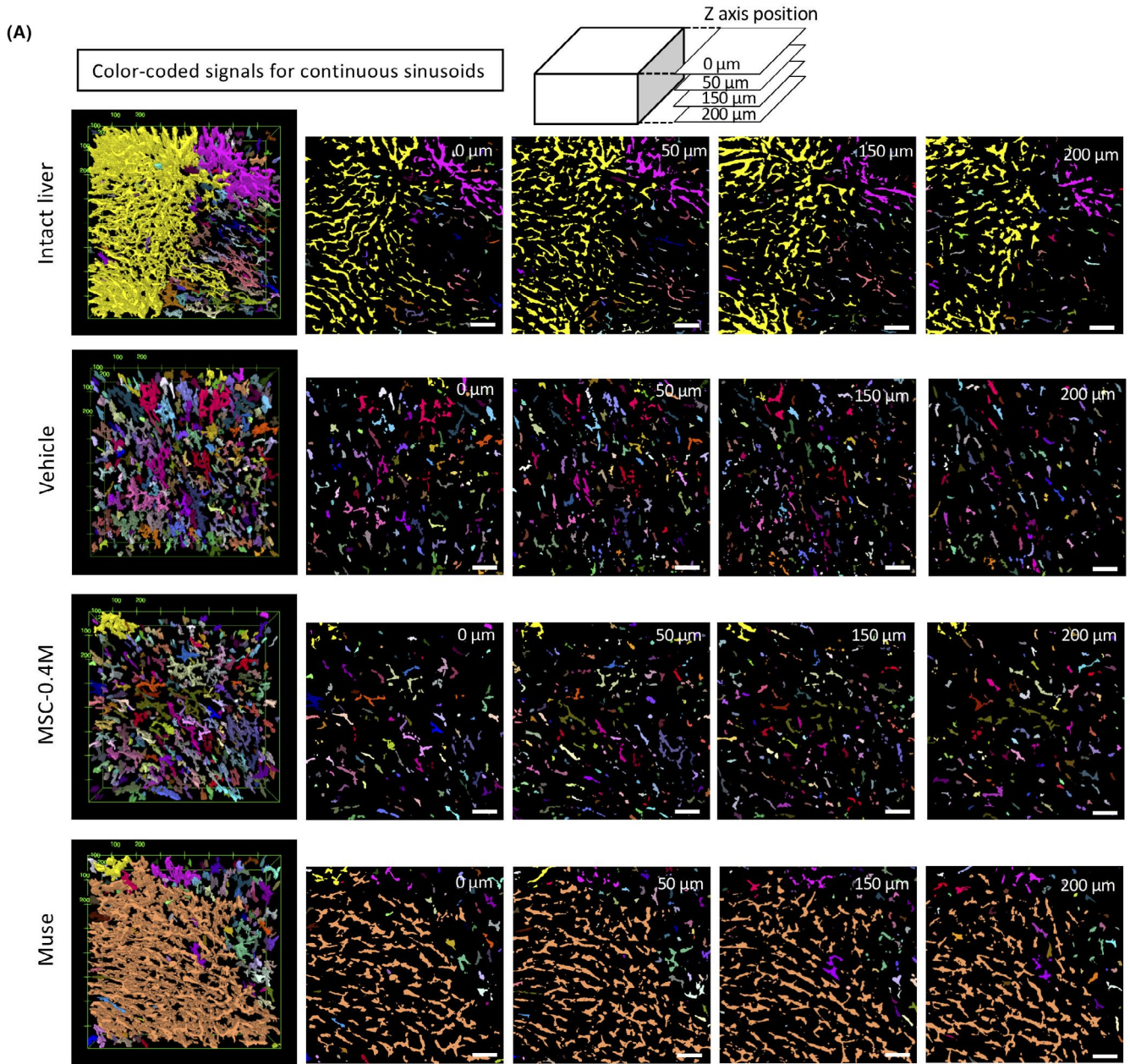Z axis position

0 μm
50 μm
150 μm
200 μm

Intact liver

Vehicle

MSC-0.4M

Muse

(B) Total liver sinusoidal volume /unit volume (%)

(C) Mean continuous sinusoidal volume (μm³)

(D) Mean continuous sinusoidal surface area (μm²)

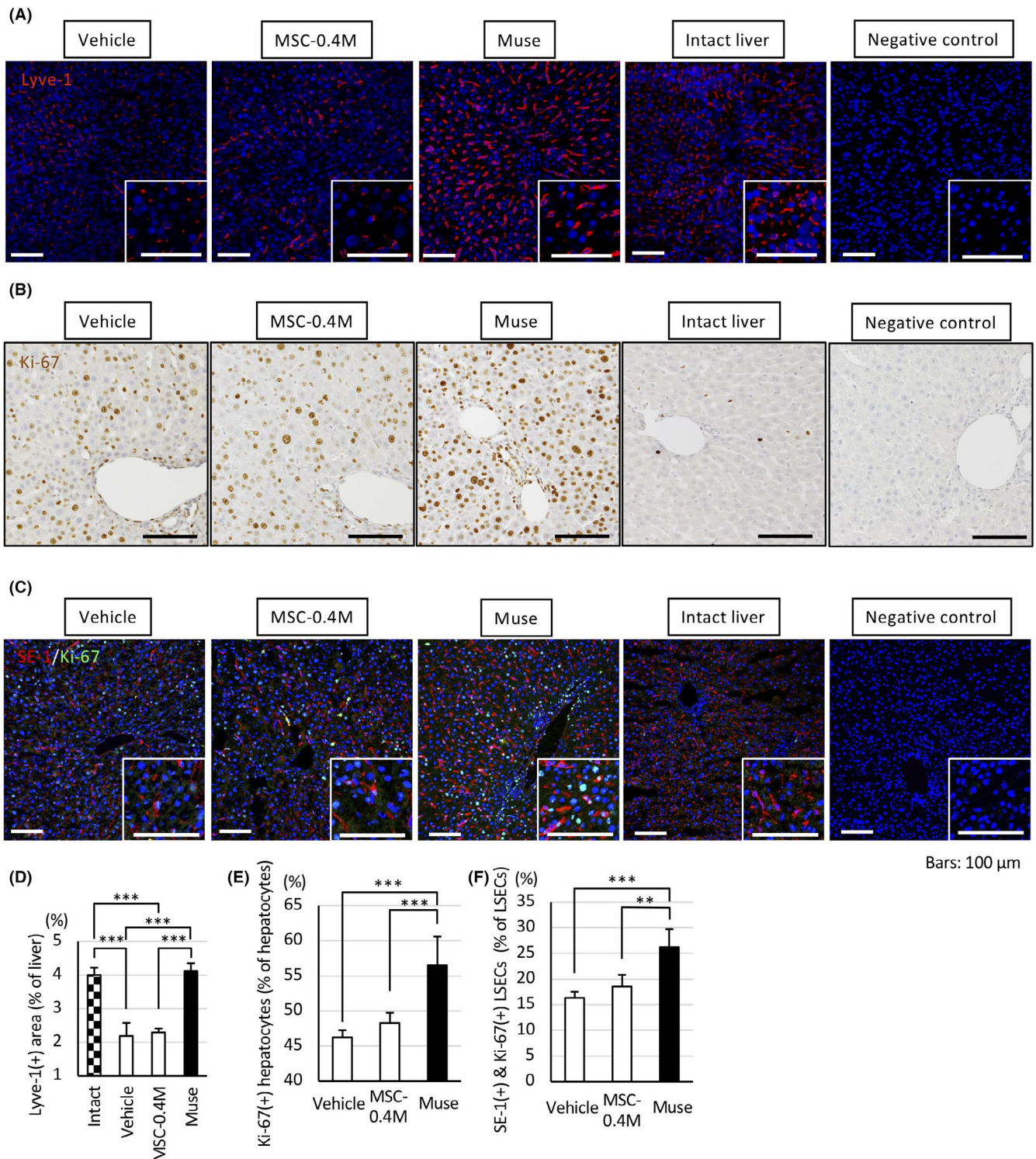**(E)** Number of interrupted sinusoids

FIGURE 6 Immunohistochemistry staining of LSECs and Ki-67. Representative images of (A) lyve-1, a surface marker for LSECs, (B) Ki-67, and (C) double staining of SE-1 (another surface marker for LSECs)/Ki-67, in each group. SE-1 and Ki-67 are stained with red and green, respectively in (C). (D) Statistical analysis revealed that the percent area positive for lyve-1 was significantly higher in the Muse group compared with the vehicle and MSC-0.4M groups. No significant difference was detected between the Muse and intact groups (10 fields/case, $n = 5$/group). (E) The percent of Ki-67(+) in hepatocytes, indicating proliferation activity, was significantly greater in the Muse group than in the vehicle and in the MSC-0.4M groups (5 fields/case, $n = 5$/group). (F) The SE-1 and Ki-67 double-positive ratio of LSECs, indicating proliferating LSECs, was significantly higher in the Muse group than in the vehicle and in the MSC-0.4M groups (10 fields/case, $n = 5$/group). Bars: 100 μm, $*p < .05$, $**p < .01$, and $***p < .001$. Ki-67, cellular proliferation marker; LSECs, liver sinusoidal endothelial cells; lyve-1, lymphatic vessel endothelial hyaluronan receptor 1; MSC, mesenchymal stem cell; Muse, multilineage-differentiating stress enduring; SE-1, hepatic sinusoidal endothelial cells

effect of Muse cells on LSECs by co-transfecting HGF- and VEGFA-small interfering RNA (siRNA; HGF/VEGF-KD-Muse cells). HGF and VEGFA levels in HGF/VEGF-KD-Muse cells were decreased to 0.072 ± 0.002 (HGF, $p < .001$) and 0.25 ± 0.004 (VEGFA, $p < .001$) times of those of naïve Muse cells (Figure 7B).

We then evaluated the ICG-PDR for the Muse and HGF/VEGF-KD-Muse groups at 3 days after injection of the cells. The HGF/VEGF-KD-Muse group had a significantly lower ICG-PDR (0.044 ± 0.016) than the Muse group (0.068 ± 0.018, $p = .0045$; Figure 7C).

The 3D images of sinusoids in the HGF/VEGF-KD-Muse group (Figure 7D, Movie S2I,J) were compared with those in the Muse group (Figures 4B and 5A, Movie S2G,H). The sinusoidal continuity observed in the Muse group was largely impaired in the HGF/VEGF-KD-Muse group (Figure 7D). In the HGF/VEGF-KD-Muse group, the total liver sinusoidal volume rate ($3.51 \pm 0.87\%$), the mean continuous sinusoidal volume ($31\,755 \pm 13\,817\,\mu m^3$), and the mean continuous sinusoid surface area ($16\,622 \pm 3831\,\mu m^2$) were significantly decreased ($p = .0001$, $<.0001$, and $<.0001$, respectively), compared with the Muse group (Figure 7E), and the values approximated those in the vehicle and MSC groups (Figure 5B–D). In contrast, the number of interrupted sinusoids in the HGF/VEGF-KD-Muse group was 299 ± 30, which was significantly higher than that in the Muse group (135 ± 30, $p < .0001$; Figure 7E).

The percent area positive for lyve-1 was lower in the HGF/VEGF-KD-Muse group ($1.21 \pm 0.06\%$) than in the Muse group ($p < .001$; Figures 6D and 7F,G). The number of Ki-67(+) hepatocytes was significantly lower in the HGF/VEGF-KD-Muse group ($36.60 \pm 3.13\%$) than in the Muse group ($p < .001$; Figures 6E and 7F, H). The SE-1 and Ki-67 double-positive ratio was significantly lower in the HGF/VEGF-KD-Muse group ($18.9 \pm 1.5\%$) than in the Muse group ($p = .0028$; Figures 6F and 7F, I).

3.8 | TUNEL staining

The TUNEL-positive cell ratio (1 ~ 2-positive cells/field) in the intact, vehicle, MSC-0.4M, and Muse groups did not differ significantly among the groups at day 3 (Figure S3).

4 | DISCUSSION

In human LDLT, the liver graft must be 30%–40% of the standard liver volume. Although our model corresponded to only 20% of the whole liver volume, the survival rate was high at day 7 without postoperative support. Furthermore, the liver graft volume was very small, and the shear stress of the LSECs was more severe than that in rat liver transplant models with larger graft sizes. Therefore, the model we used was not identical to clinical SFSS but may mimic the pathology of sinusoidal dysfunction after liver transplantation.

Human Muse cells preferentially accumulated to the grafted liver after intravenous injection, and delivered LSEC protection as represented by well-organized sinusoid continuity compared with the vehicle and MSC-0.4M groups. Concomitantly, the indicators of liver function, ICG-PDR, AST, and ALT, were improved, and the amount of Ki-67(+)-hepatocytes and -LSECs, suggesting proliferating hepatocytes and LSECs, was higher in the Muse group. Thus, the grafted liver was suggested to be less damaged in the Muse group than in the other two groups. These beneficial effects were abolished when HGF and VEGFA expression was knocked down in the Muse cells, suggesting a role for these two factors in the LSEC protection effect of Muse cells. Compared with MSCs, Muse cells expressed higher HGF and VEGFA levels and intensively homed to the grafted liver after intravenous injection, where they might have successfully delivered HGF and VEGFA to the LSEC in the grafted liver.

In the Muse group, the sinusoid patency and continuity were improved and the amount of LSECs assessed by lyve-1 immunostaining was higher than that in the vehicle and MSC-0.4M groups. Furthermore, Muse cells appeared to accelerate the proliferation of both hepatocytes and LSECs.

Notably, both the mean continuous sinusoidal volume and mean surface area were higher in the Muse group than in the intact group. The sinusoids of the intact liver appeared thinner and less continuous than those in the Muse group, which might be explained by the enlargement and extension of the grafted liver due to portal hypertension, leading to sinusoidal expansion in the Muse group.

The MSC-5M group contained the same absolute number of Muse cells as the Muse group. Despite the same number of Muse cells, the MSC-5M group had a significantly lower ICG-PDR than the Muse group. In addition, the Muse group exhibited significantly better recovery of AST and ALT than the vehicle group, but these beneficial effects were not observed in the MSC-5M group. In fact, the accumulation of Akaluc-MSCs was lower than that of Muse cells in the grafted liver after intravenous injection, and expression of HGF and VEGFA was lower than that in the Muse group. The majority of MSCs comprise a non-Muse population, and thus the beneficial effects delivered by a small subpopulation of Muse cells were likely diluted in the MSC-5M group. MSCs have not only anti-inflammatory effects, but also pro-inflammatory effects.[49] Thus, the majority portion of MSCs may offset the beneficial effects of the Muse cells.

Administration of a smaller number of cells may decrease the risk of pulmonary embolism.[50] Therefore, from the perspective of both protective effects and pulmonary embolism, a smaller cell number with a higher Muse cell ratio has greater advantages than a large number of MSCs, despite containing the same number of Muse cells, for systemic administration.

In the clinical situation, LDLT is performed for patients with liver cirrhosis and multiple organ disorders, including kidney injury, pulmonary shunting, and cardiac remodeling. Muse cells may home to the liver as well as to other damaged organs via the S1P-S1PR2 axis
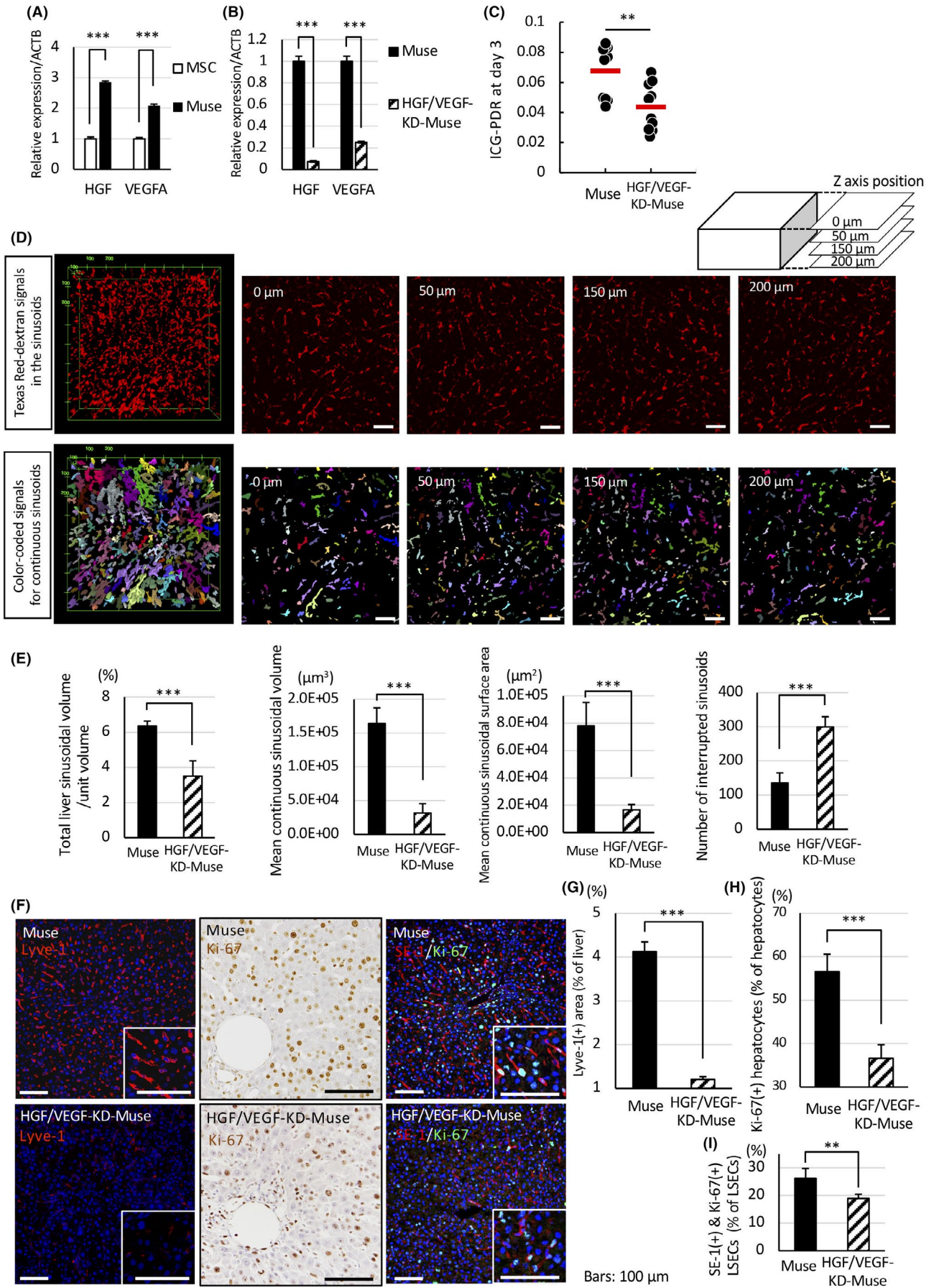
Bars: 100 μm

FIGURE 7 Muse cells co-transfected with siRNA for HGF and VEGFA. (A) Gene expression levels of HGF and VEGFA were substantially higher in Muse cells than in MSCs in qPCR. (B) Co-transfection of Muse cells with HGF- and VEGFA-siRNA significantly suppressed HGF and VEGF expression in qPCR. (C) ICG-PDR in the Muse and HGF/VEGF-KD-Muse groups 3 days after cell injection. The HGF/VEGF-KD-Muse group had a significantly lower ICG-PDR than the Muse group. (D) Representative liver sinusoidal 3D frames of movies and 2D images exported from 3D images in the HGF/VEGF-KD-Muse group (Texas Red-dextran signals and color-coded signals of sinusoids). (E) Liver sinusoid morphologic data. In the HGF/VEGF-KD-Muse group, total liver sinusoidal volume rate, mean continuous sinusoidal volume, and mean continuous sinusoidal surface area were all significantly decreased compared with the Muse group ($n = 5$/group). In contrast, the number of interrupted sinusoids was significantly higher in the HGF/VEGF-KD-Muse group than in the Muse group. (F) From the left, lyve-1 staining in the Muse and HGF/VEGF-KD-Muse groups, Ki-67, and double staining for SE-1/ Ki-67. (G) The percent area positive for lyve-1 was lower in the HGF/VEGF-KD-Muse group than in the Muse group (10 fields/case, $n = 5$/group). (H) The ratio of Ki-67(+)-hepatocytes was significantly lower in the HGF/VEGF-KD-Muse group than in the Muse group (5 fields/case, $n = 5$/group). (I) The ratio of SE-1(+)/Ki-67(+) LSECs was significantly lower in the HGF/VEGF-KD-Muse group than in the Muse group (10 fields/case, $n = 5$/group). The size of the rectangle in the 3D snapshots is X: 795.5 µm × Y: 795.5 µm × Z: 200.6 µm. Bars: 100 µm, $*p < .05$, $**p < .01$, and $***p < .001$. 2D, two-dimensional; 3D, three-dimensional; ACTB, beta actin; HGF, hepatocyte growth factor; HGF/VEGF-KD-Muse, HGF/VEGFA-knocked down-Muse cells; ICG-PDR, indocyanine green-plasma disappearance rate; MSC, mesenchymal stem cell; Muse, multilineage-differentiating stress enduring; RNA, ribonucleic acid; siRNA, small interfering ribonucleic acid; VEGFA, vascular endothelial growth factor A

when systemically administered to patients with liver cirrhosis.[31,51] The number of Muse cells required to treat patients should be re-estimated based on liver transplantation experiments in animal models of cirrhosis.

The siRNA experiment suggested that HGF and VEGFA are major factors involved in the LSEC protective effects of Muse cells. This raises the question of whether administering HGF and VEGF would have the same effects. There are several reports of the administration of recombinant HGF or VEGF, or MSCs genetically modified to express high levels of HGF or VEGF.[13,52-55] Generally, recombinant factors degrade quickly and require frequent repetitive administration, making the dosing difficult to control.[53,55] Furthermore, administration of genetically modified cells to humans is associated with safety concerns.[56] Muse cells originally express higher levels of HGF and VEGF than MSCs, and there is thus no need for gene transfer.

Muse cell clinical trials based on intravenous administration of donor-derived Muse cells without HLA-matching or immunosuppressant administration have been conducted for several diseases.[36,37] While careful validation must be continued in preclinical studies, the advantageous properties of Muse cells might be applicable to SFSS. As demonstrated in this study, a reduced number of Muse cells can be administered compared with MSCs, and this may contribute to reduce the burden on patients with SFSS.

Improvement of the sinusoidal condition contributes to postoperative liver regeneration and can be expected to reduce SFSS. The results of the present study suggest that a new technique called hybrid liver-cell transplantation, which combines cell transplantation using Muse cells and organ transplantation of small-for-size grafts, is expected to be an effective treatment for end-stage liver disease.

DISCLOSURE

The authors of this manuscript have conflicts of interest to disclose as described by the *American Journal of Transplantation*. Yoshihiro Kushida, Shohei Wakao, Yasumasa Kuroda, and Mari Dezawa are parties to a co-development and co-research agreement with Life Science Institute, Inc. (LSII: Tokyo, Japan). Mari Dezawa and Shohei Wakao have a patent for Muse cells, and the Muse cell isolation method is licensed to LSII. Yoshihiro Kushida, Shohei Wakao, Yasumasa Kuroda, and Mari Dezawa received a joint research grant from LSII.

DATA AVAILABILITY STATEMENT

Research data are not shared.

ORCID

Yoshihiro Shono https://orcid.org/0000-0002-0804-285X
Yoshihiro Kushida https://orcid.org/0000-0002-5840-5292
Michiaki Unno https://orcid.org/0000-0002-2145-6416
Takashi Kamei https://orcid.org/0000-0003-1282-0463
Shigehito Miyagi https://orcid.org/0000-0002-7628-3487
Mari Dezawa https://orcid.org/0000-0001-9978-6178

REFERENCES

1. Burra P, Freeman R. Trends in liver transplantation 2011. *J Hepatol*. 2012;56(Suppl 1):S101-S111.
2. Makuuchi M. Living donor liver transplantation: looking back at my 30 years of experience. *Surg Today*. 2019;49(4):288-294.
3. Kim PTW, Testa G. Living donor liver transplantation in the USA. *Hepatobiliary Surg Nutr*. 2016;5(2):133-140.
4. Sudhindran S, Menon RN, Balakrishnan D. Challenges and outcome of left-lobe liver transplants in adult living donor liver transplants. *J Clin Exp Hepatol*. 2012;2(2):181-187.
5. Yagi S, Uemoto S. Small-for-size syndrome in living donor liver transplantation. *Hepatobiliary Pancreat Dis Int*. 2012;11(6): 570-576.

6. Wang HS, Ohkohchi N, Enomoto Y, et al. Excessive portal flow causes graft failure in extremely small-for-size liver transplantation in pigs. *World J Gastroenterol*. 2005;11(44):6954-6959.

7. Gruttadauria S, Mandala L, Miraglia R, et al. Successful treatment of small-for-size syndrome in adult-to-adult living-related liver transplantation: single center series. *Clin Transplant*. 2007;21(6):761-766.

8. Humar A, Beissel J, Crotteau S, et al. Delayed splenic artery occlusion for treatment of established small-for-size syndrome after partial liver transplantation. *Liver Transpl*. 2009;15(2):163-168.

9. Kinaci E, Kayaalp C. Portosystemic shunts for "too small-for-size syndrome" after liver transplantation: a systematic review. *World J Surg*. 2016;40(8):1932-1940.

10. Shoreem H, Gad EH, Soliman H, et al. Small for size syndrome difficult dilemma: Lessons from 10 years single centre experience in living donor liver transplantation. *World J Hepatol*. 2017;9(21):930-944.

11. Hessheimer AJ, Martínez de la Maza L, Adel Al Shwely F, et al. Somatostatin and the "small-for-size" liver. *Int J Mol Sci*. 2019;20(10):2512.

12. Wang W, Du Z, Yan J, et al. Mesenchymal stem cells promote liver regeneration and prolong survival in small-for-size liver grafts: Involvement of C-Jun N-terminal kinase, cyclin D1, and NF-kappaB. *PLoS One*. 2014;9(12):e112532.

13. Ma T, Liu H, Chen W, et al. Implanted adipose-derived stem cells attenuate small-for-size liver graft injury by secretion of VEGF in rats. *Am J Transplant*. 2012;12(3):620-629.

14. Gao W, Zhang L, Zhang Y, et al. Adipose-derived mesenchymal stem cells promote liver regeneration and suppress rejection in small-for-size liver allograft. *Transpl Immunol*. 2017;45:1-7.

15. Kim T, Mars WM, Stolz DB, et al. Extracellular matrix remodeling at the early stages of liver regeneration in the rat. *Hepatology*. 1997;26(4):896-904.

16. Streetz KL, Luedde T, Manns MP, et al. Interleukin 6 and liver regeneration. *Gut*. 2000;47(2):309.

17. Taki-Eldin A, Zhou L, Xie HY, et al. Liver regeneration after liver transplantation. *Eur Surg Res*. 2012;48(3):139-153.

18. van de Laarschot LFM, Jansen PLM, Schaap FG, et al. The role of bile salts in liver regeneration. *Hepatol Int*. 2016;10(5):733-740.

19. Huang J, Rudnick DA. Elucidating the metabolic regulation of liver regeneration. *Am J Pathol*. 2014;184(2):309-321.

20. Preziosi ME, Monga SP. Update on the mechanisms of liver regeneration. *Semin Liver Dis*. 2017;37(2):141-151.

21. Li J, Liang L, Ma T, et al. Sinusoidal microcirculatory changes after small-for-size liver transplantation in rats. *Transplant Int*. 2010;23(9):924-933.

22. Poisson J, Lemoinne S, Boulanger C, et al. Liver sinusoidal endothelial cells: physiology and role in liver diseases. *J Hepatol*. 2017;66(1):212-227.

23. Braet F, Shleper M, Paizi M, et al. Liver sinusoidal endothelial cell modulation upon resection and shear stress in vitro. *Comp Hepatol*. 2004;3(1):7.

24. Yamanaka K, Hatano E, Narita M, et al. Olprinone attenuates excessive shear stress through up-regulation of endothelial nitric oxide synthase in a rat excessive hepatectomy model. *Liver Transpl*. 2011;17(1):60-69.

25. Kuroda Y, Kitada M, Wakao S, et al. Unique multipotent cells in adult human mesenchymal cell populations. *Proc Natl Acad Sci USA*. 2010;107(19):8639-8643.

26. Leng Z, Sun D, Huang Z, et al. Quantitative analysis of SSEA3+ cells from human umbilical cord after magnetic sorting. *Cell Transplant*. 2019;28(7):907-923.

27. Dezawa M. Muse cells provide the pluripotency of mesenchymal stem cells: direct contribution of Muse cells to tissue regeneration. *Cell Transplant*. 2016;25(5):849-861.

28. Tanaka T, Nishigaki K, Minatoguchi S, et al. Mobilized Muse cells after acute myocardial infarction predict cardiac function and re-modeling in the chronic phase. *Circ J*. 2018;82(2):561-571.

29. Kuroda Y, Dezawa M. Mesenchymal stem cells and their subpopulation, pluripotent Muse cells, in basic research and regenerative medicine. *Anat Rec*. 2014;297(1):98-110.

30. Fisch SC, Gimeno ML, Phan JD, et al. Pluripotent nontumorigenic multilineage differentiating stress enduring cells (Muse cells): a seven-year retrospective. *Stem Cell Res Ther*. 2017;8(1):227.

31. Yamada Y, Wakao S, Kushida Y, et al. S1P–S1PR2 axis mediates homing of Muse cells into damaged heart for long-lasting tissue repair and functional recovery after acute myocardial infarction. *Circ Res*. 2018;122(8):1069-1083.

32. Iseki M, Kushida Y, Wakao S, et al. Muse cells, nontumorigenic pluripotent-like stem cells, have liver regeneration capacity through specific homing and cell replacement in a mouse model of liver fibrosis. *Cell Transplant*. 2017;26(5):821-840.

33. Katagiri H, Kushida Y, Nojima M, et al. A distinct subpopulation of bone marrow mesenchymal stem cells, Muse cells, directly commit to the replacement of liver components. *Am J Transplant*. 2016;16(2):468-483.

34. Hosoyama K, Wakao S, Kushida Y, et al. Intravenously injected human multilineage-differentiating stress-enduring cells selectively engraft into mouse aortic aneurysms and attenuate dilatation by differentiating into multiple cell types. *J Thorac Cardiovasc Surg*. 2018;155(6):2301-2313 e2304.

35. Yabuki H, Wakao S, Kushida Y, et al. Human multilineage-differentiating stress-enduring cells exert pleiotropic effects to ameliorate acute lung ischemia-reperfusion injury in a rat model. *Cell Transplant*. 2018;27(6):979-993.

36. Dezawa M. Clinical trials of Muse cells. *Adv Exp Med Biol*. 2018;1103:305-307.

37. Noda T, Nishigaki K, Minatoguchi S. Safety and efficacy of human Muse cell-based product for acute myocardial infarction in a first-in-human trial. *Circ J*. 2020;84(7):1189-1192.

38. Ito T, Kiuchi T, Yamamoto H, et al. Changes in portal venous pressure in the early phase after living donor liver transplantation: pathogenesis and clinical implications. *Transplantation*. 2003;75(8):1313-1317.

39. Tanaka H, Hashizume K, Enosawa S, et al. Successful transplantation of a 20% partial liver graft in rats: a technical innovation. *J Surg Res*. 2003;110(2):409-412.

40. Kubota T, Takabe K, Yang M, et al. Minimum sizes for remnant and transplanted livers in rats. *J Hepatobiliary Pancreat Surg*. 1997;4(4):398-404.

41. Uchida H, Niizuma K, Kushida Y, et al. Human Muse cells reconstruct neuronal circuitry in subacute lacunar stroke model. *Stroke*. 2017;48(2):428-435.

42. Alessio N, Squillaro T, Özcan S, et al. Stress and stem cells: adult Muse cells tolerate extensive genotoxic stimuli better than mesenchymal stromal cells. *Oncotarget*. 2018;9(27):19328-19341.

43. Maida K, Akamatsu Y, Hara Y, et al. Short oxygenated warm perfusion with prostaglandin E1 administration before cold preservation as a novel resuscitation method for liver grafts from donors after cardiac death in a rat in vivo model. *Transplantation*. 2016;100(5):1052-1058.

44. Kamada N, Calne RY. Orthotopic liver transplantation in the rat. Technique using cuff for portal vein anastomosis and biliary drainage. *Transplantation*. 1979;28(1):47-50.

45. Hori T, Gardner LB, Chen F, et al. Impact of hepatic arterial reconstruction on orthotopic liver transplantation in the rat. *J Invest Surg*. 2012;25(4):242-252.

46. de Graaf W, Bennink RJ, Heger M, et al. Quantitative assessment of hepatic function during liver regeneration in a standardized rat model. *J Nucl Med*. 2011;52(2):294-302.

47. Iwano S, Sugiyama M, Hama H, et al. Single-cell bioluminescence imaging of deep tissue in freely moving animals. *Science*. 2018;359(6378):935-939.

48. LeCouter J, Moritz DR, Li B, et al. Angiogenesis-independent endothelial protection of liver: role of VEGFR-1. *Science*. 2003;299(5608):890-893.

49. Avery MB, Belanger BL, Bromley A, et al. Mesenchymal stem cells exhibit both a proinflammatory and anti-inflammatory effect on saccular aneurysm formation in a rabbit model. *Stem Cells Int*. 2019;2019:3618217.

50. Liao L, Shi B, Chang H, et al. Heparin improves BMSC cell therapy: anticoagulant treatment by heparin improves the safety and therapeutic effect of bone marrow-derived mesenchymal stem cell cytotherapy. *Theranostics*. 2017;7(1):106-116.

51. Uchida N, Kushida Y, Kitada M, et al. Beneficial effects of systemically administered human Muse cells in adriamycin nephropathy. *J Am Soc Nephrol*. 2017;28(10):2946-2960.

52. Adas G, Koc B, Adas M, et al. Effects of mesenchymal stem cells and VEGF on liver regeneration following major resection. *Langenbecks Arch Surg*. 2016;401(5):725-740.

53. Ishii T, Sato M, Sudo K, et al. Hepatocyte growth factor stimulates liver regeneration and elevates blood protein level in normal and partially hepatectomized rats. *J Biochem*. 1995;117(5):1105-1112.

54. Zhang Y, Li R, Rong W, et al. Therapeutic effect of hepatocyte growth factor-overexpressing bone marrow-derived mesenchymal stem cells on CCl4-induced hepatocirrhosis. *Cell Death Dis*. 2018;9(12):1186.

55. Bockhorn M, Goralski M, Prokofiev D, et al. VEGF is important for early liver regeneration after partial hepatectomy. *J Surg Res*. 2007;138(2):291-299.

56. Han J, Liu Y, Liu H, et al. Genetically modified mesenchymal stem cell therapy for acute respiratory distress syndrome. *Stem Cell Res Ther*. 2019;10(1):386.

SUPPORTING INFORMATION

Additional supporting information may be found online in the Supporting Information section.